Nonlinear Dyn (2016) 85:1297–1318
DOI 10.1007/s11071-016-2761-x

ORIGINAL PAPER

An evaluation of data-driven identification strategies for complex nonlinear dynamic systems

Patrick T. Brewick · Sami F. Masri

Received: 28 July 2015 / Accepted: 24 March 2016 / Published online: 5 April 2016

Abstract The development of suitable mathematical models on the basis of dynamic measurements from dispersed structural systems that may be undergoing significant nonlinear behavior is an important and very challenging problem in the field of Applied Mechanics that has drawn the attention of numerous investigators and motivated the development of many approaches for extracting reduced-order, reduced-complexity models from such systems. However, even though numerous nonlinear system identification techniques that are focused on the class of problems encountered in the structural dynamics field have been developed over the past decades, there are no systematic studies available that rigorously compare the performance and fidelity of such methods under similar operating conditions, and when encountering challenging nonlinear phenomena (such as hysteresis) that are present in physical systems, at different scales. This paper explores a variety of data-driven identification techniques for complex nonlinear systems and provides a much needed critical comparison of the accuracy and performance of each method. The Volterra/Wiener neural network (VWNN), a more recent development in nonlinear identification, is featured and compared against several existing methods, including polynomial-based nonlinear estimators and other artificial neural network systems. A representative three degree-of-freedom structure with nonlinear restoring force elements is used as the primary means of comparison for the different methods, and a variety of nonlinear models were investigated, including bilinear hysteresis, polynomial stiffness, and Bouc–Wen hysteresis. Performance comparisons were based on the ability to estimate the acceleration responses for both training and testing simulations. The results showed that, in general, the VWNN provided better accuracy in its estimates for each model. The VWNN also performed best when evaluated for scenarios in which numerical integration is required to find velocity and displacement information from measured accelerations or sensor noise is present in the measured responses.

Keywords Nonlinear identification · Data-driven methods · Neural networks · Bouc–Wen · Hysteresis

P. T. Brewick (✉) · S. F. Masri
Viterbi School of Engineering, University of Southern California, Los Angeles, CA 90089, USA
e-mail: brewick@usc.edu

1 Introduction

1.1 Motivation

With the explosive growth in available data from dynamic systems encountered in the broad field of Applied Mechanics, there is a growing interest in the development and application of sophisticated data-based procedures to identify the properties of such systems through the identification of reduced-order, reduced-complexity mathematical models that can be used for active control applications, computational sim-

ulations, or for structural health monitoring methodologies based on vibration signature analysis. While the field of system identification of linear systems is a very well-developed and mature topic (with strong roots in the digital signal processing field), in which a variety of powerful time-domain and frequency-domain approaches have been established and widely applied [2,9,19,22,27,30,48,51,56], there is a paucity of similar approaches that deal with nonlinear systems typically encountered in the field of structural dynamics, at many scales.

The behavior and modeling of nonlinear systems has been the subject of seminal works on bilinear hysteresis [10], yielding structures [29], degrading systems [5,6] and other hysteretic systems and structures [8,24,26,40,58]. A helpful survey of Bouc–Wen hysteretic models [59], a particular class of nonlinear models, may be found in [23]. These various models have continued to advance [3,4,17,39,45,57,64], better capturing the complexities of different nonlinearities, but the identification of these systems remains a work-in-progress.

In part, the degree of difficulty is so high for nonlinear system identification approaches because, as good as models may be at capturing nonlinear phenomena, the nonlinear physical behavior actually encountered in real-world structures and systems is not of course governed exactly by these equations and models. Several contributions have been made using parametric identification methods for various models, including: single-valued models [1], distributed element models [25], Masing models [28], modal models [50], wavelets [20], and the Bouc–Wen model. The Bouc–Wen, in particular, has seen its parameters estimated via nonlinear optimization schemes, [65], Bayesian state estimate with bootstrap filters [34], adaptive on-line methods [11,12,52], and applications of the extended Kalman filter (EKF) [21,38,63,66] and the unscented Kalman filter [13,14,61]. Despite the differences in these approaches, they all require some assumption about the form or characterization of the nonlinearity.

One of the significant hurdles in the development of mathematical models on the basis of vibration data extracted from systems undergoing significant nonlinear deformations is the initial step of selecting the ***model class*** to identify, before proceeding to determine the optimum values for the parameters of the selected model. The more complex (and realistic) the choice of nonlinear models become, the more challenging it becomes to select the appropriate phenomenological model to identify. This serious difficulty in the use of parametric identification approaches progressively worsens when the target system of interest is dispersed in nature or has challenging nonlinear features (e.g., hysteresis, limited slip, distributed plastic deformations, multi-component frictional effects, etc.) to be captured with sufficient fidelity.

The above-mentioned serious limitation of parametric nonlinear system identification approaches, has motivated the development of variety of methods and approaches that are referred to as nonparametric, or model-free, identification methods because they use various basis functions to represent the nonlinear system. Some nonparametric methods include the use of Chebyshev polynomials [42], least square methods [43,44], power series basis functions [41,46], and other polynomial functions [55]. Nonparametric techniques have the advantage of remaining agnostic about the particular manifestation of the nonlinearity and instead use a set of basis functions to create a nonlinear representation of the observed system. Basis functions often utilize different measured response quantities, and for this reason, these methods are sometimes referred to as data-driven, or data-based, identification. The applications for nonparametric methods has been expanded to include identification for hysteretic systems under earthquake loading [7] and structural health monitoring and damage detection [36,54]. Some of the more recent developments in nonparametric identification have focused on using various neural network architectures [15,16,33,35,37,49,62]. Among these advancements, the Volterra/ Wiener neural network (VWNN) [33] has shown some particular promise for accurate nonlinear identification.

Given the extremely wide variety of situations that are encountered in real-life structural dynamics applications (e.g., the many types of physical systems that differ in material properties, level of nonlinearity, nonlinear phenomenological features of interest, topology of dispersed systems, degrees-of-freedom, sensing modalities, knowledge of the dynamic loads, spectral content of the excitation, physical scale of the system, stationarity of the system and/or the excitation, etc.), it is obvious that no one method would be expected to perform well for all conceivable situations. Consequently, over the past few decades, researchers have developed a collection of methods, each with its own

strengths and limitations, that are each optimized for certain situations of interest to the Applied Mechanics community. A review of nonlinear system identification within structural dynamics has been compiled in [31].

With the above in mind, the main goal of the present study is to conduct a "fair" comparison of the leading nonparametric nonlinear system identification techniques that have been widely used for a variety of applications. Different polynomial basis functions, specifically power series [41,46] and Chebyshev polynomials [42], and neural network approaches, both artificial neural networks (ANNs) [15,16] and the VWNN [33], will be investigated in the present study. Each of these methods includes its own parameters to "tune," such as the order, or degree, of the polynomial and number of neurons in a layer. The comparison will be based on evaluating their performance and robustness in accurately capturing the dominant features of a calibration multi-degree-of-freedom (MDOF) system that many other investigators have previously used to assess the utility of some proposed identification schemes.

1.2 Scope

In this paper, the performance of the VWNN is evaluated through comparisons to several other leading nonparametric identification methods for nonlinear systems. This paper highlights the advantages of the VWNN method for identification due to its limited reliance on response information (only accelerations and excitations are required) and its widespread applicability for nonlinear systems by evaluating it through three different models, namely bilinear hysteresis, polynomial nonlinearity, and Bouc–Wen hysteresis.

The paper is organized as follows: Sect. 2 provides the formulation and background for the nonlinear identification techniques considered herein, Sect. 3 presents the nonlinear models included in this study as well as the chosen parameters for the different identification techniques, and Sect. 4 includes the results for the applications of each of the identification methods as well as an extended discussion of their accuracy and effectiveness for systems with limited response information and noisy measurements. A summary of the results and future research needs are provided in Sect. 5.

2 Nonlinear identification strategies

The generic equation of motion for a multi-degree-of-freedom (MDOF) system subjected to external excitation forces is given by Eq. 1:

$$\mathbf{M}\ddot{\mathbf{x}}(t) + \mathbf{r}\left(\dot{\mathbf{x}}(t), \mathbf{x}(t), \mathbf{p}\right) = \mathbf{f}(t) \tag{1}$$

where $\mathbf{M}$ is the constant mass matrix, $\mathbf{x}(t)$ is the displacement vector, $\mathbf{f}(t)$ is the column vector of externally applied forces, and $\mathbf{r}\left(\dot{\mathbf{x}}(t), \mathbf{x}(t), \mathbf{p}\right)$ represents the restoring force vector. (The vectors within this paper are column vectors unless otherwise noted.) The restoring force vector contains both linear conservative and nonlinear non-conservative forces. The vector $\mathbf{p}$ represents the system-specific parameters related to the restoring forces.

For the purposes of identification, the equation of motion in Eq. 1 may be reorganized to isolate the accelerations:

$$\ddot{\mathbf{x}}(t) = -\mathbf{M}^{-1}\mathbf{r}\left(\dot{\mathbf{x}}(t), \mathbf{x}(t), \mathbf{p}\right) + \mathbf{M}^{-1}\mathbf{f}(t) \tag{2}$$

Since the individual elements within the restoring force vector, such as the damping, stiffness, and hysteretic functions, are unknown, only their *combined* effects can be estimated. Therefore, instead of trying to estimate all of the individual restoring force terms within $\mathbf{r}\left(\dot{\mathbf{x}}(t), \mathbf{x}(t), \mathbf{p}\right)$ of Eq. 2, the various nonlinear identification techniques considered in the present study will seek to directly estimate $\ddot{\mathbf{x}}(t)$. Note that the knowledge of $\ddot{\mathbf{x}}(t)$ allows its utilization in conjunction with time-marching techniques for computational simulation studies.

Specifically, this study will consider the Volterra/Wiener neural network, power series and Chebyshev polynomial estimators, and artificial neural network approaches for nonlinear identification. Brief reviews of the inner workings of these methods will be presented in the following subsections to facilitate discussions of performance and comparisons among methods.

2.1 Volterra/Wiener neural network

The Volterra/Wiener neural network (VWNN) [33] does not assume any particular model for the system to be identified. Rather the VWNN operates in a similar manner to other artificial neural networks in that identification is a purely input–output process. The

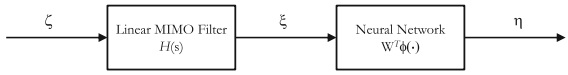

Fig. 1 Block diagram of Volterra/Wiener neural network

VWNN consists of a linear multi-input multi-output (MIMO) style dynamical system connected in cascade with a linear-in-the-weights neural network, as shown in Fig. 1. The general description of the MIMO dynamical system is given in Eq. 3, where ζ is the input, $H(s)$ is a stable transfer function matrix (s denotes a Laplace operator) and ξ is a the output of the linear MIMO system:

$$\xi = H(s)\zeta \tag{3}$$

The linear-in-the-weights neural network is described by Eq. 4:

$$\eta = W^{\mathrm{T}}\phi\left(\xi\right) = \hat{\ddot{\mathbf{x}}}(t) \tag{4}$$

where $\phi\left(\cdot\right)$ is the vector of nonlinear activation functions of the neural network, W is the matrix of synaptic weights of the neural network, and η is the output of the neural network. A more detailed explanation of linear-in-the-weights neural networks and the VWNN may be found in [33].

Ultimately, the VWNN is used to approximate the acceleration vector $\ddot{\mathbf{x}}(t)$ using the relationship given by 5. The vector θ contains the same values as the neural network weight matrix W except that the weights have been concatenated into a single column vector. The term ϵ represents the modeling error, which measures how closely the VWNN approximates the measured acceleration for a given DOF:

$$\ddot{x}_i = \theta^{\mathrm{T}}\phi\left(\xi\right) + \epsilon \tag{5}$$

where $\ddot{x}_i$ is the acceleration of the ith DOF within vector $\ddot{\mathbf{x}}$.

The original inputs for the VWNN are chosen as $\zeta = [\ddot{\mathbf{x}}(t), \mathbf{f}(t)]^{\mathrm{T}}$. This assumes that the response accelerations may be measured at each DOF and that the external excitations have been measured. The original inputs are passed through the MIMO dynamical system, which involves a series of transfer functions. Low-pass filters are used for the transfer functions. The filtering is applied in a cascading process.

In order to properly capture the possible nonlinear dynamics of a given structural system, a high-order neural network (HONN) (as described in [32]) is chosen for the activation function ϕ. The HONN passes the modified input vector ξ through a hyperbolic tangent sigmoidal function, and the resulting output forms the first entries of ϕ, which are deemed first-order terms. The work in [49] recommends a hyperbolic tangent sigmoidal with zero bias and a uniform weight λ applied to all inputs, as shown in Eq. 6:

$$h\left(p\right) = \frac{2}{1 + \mathrm{e}^{-2\lambda p}} - 1 \tag{6}$$

where $h\left(p\right)$ represents a first-order term in the vector ϕ and p represents an input from the vector ξ. The appropriate value for λ depends heavily on the input range for p [49]. The vector ϕ is then augmented with higher-order terms by adding all of the unique products between two individual first-order entries in ϕ. These are referred to as second-order terms, but additional higher-order terms may be similarly computed.

The weights θ of the VWNN may be estimated using linear least squares. In previous implementations of the VWNN, on-line adaptive estimation has been used to drive the estimation of the weights [33]. However, the present study does not focus on on-line estimation techniques and instead presents a novel application of the VWNN for batch identification. Since the VWNN is a linear-in-the-weights neural network, using a least squares approach will produce the optimal estimates for the weights.

2.2 Polynomial basis methods

For these methods, the linear contribution to the equation of motion in Eq. 1 is first identified by using a time-domain method to generate the equivalent linear system matrices. This is accomplished by re-writing Eq. 2 as the follows:

$$\ddot{\mathbf{x}}(t) = -\mathbf{M}^{-1}\mathbf{C}\dot{\mathbf{x}}(t) - \mathbf{M}^{-1}\mathbf{K}\mathbf{x}(t) + \mathbf{M}^{-1}\mathbf{f}(t) \tag{7}$$

where $\mathbf{C}$ and $\mathbf{K}$ are constant matrices that provide an equivalent linearized damping and stiffness, respectively. Assuming that the accelerations, displacements, velocities, and externally applied forces are available, the acceleration of the ith DOF may be re-written as:

$$\ddot{x}_i(t) = \sum_{j=1}^{n} a_{ij}\dot{x}_j(t) + \sum_{j=1}^{n} b_{ij}x_j(t) + \sum_{j=1}^{n} c_{ij}f_j(t) \qquad i = 1, 2, \ldots, n \tag{8}$$

where a_{ij}, b_{ij}, and c_{ij} are elements of the unknown system matrices $-\mathbf{M}^{-1}\mathbf{C}$, $-\mathbf{M}^{-1}\mathbf{K}$, and $-\mathbf{M}^{-1}$, respectively. (It may be assumed that the accelerations and

forces are available from measurements, whereas the displacements and velocities may come directly from measurements or indirectly through integration of the measured accelerations.) Further, these are linear coefficients that may be solved for using standard least squares techniques. Once these matrices have been estimated, the nonlinear aspect of the system may be determined in one of two ways.

The first approach assumes that the residual between the equivalent linear system and the measured accelerations represents the nonlinear contribution to the response $\mathbf{f}_{NL}(t)$, as shown in Eq. 9:

$$\mathbf{f}_{NL}(t) = \mathbf{f}(t) - (\mathbf{M}\ddot{\mathbf{x}}(t) + \mathbf{C}\dot{\mathbf{x}}(t) + \mathbf{K}\mathbf{x}(t)) \tag{9}$$

The other approach relies upon using the identified mass matrix to determine the unknown nonlinear restoring force according to Eq. 10:

$$\mathbf{r}(t) = \mathbf{f}(t) - \mathbf{M}\ddot{\mathbf{x}}(t) \tag{10}$$

For both of these methods, the next step is to fit a polynomial function in order to capture the nonlinear behavior of the system. However, it has been shown that is more efficient to "rotate" the system coordinates using the eigenvectors corresponding to the linearized system matrices [41,46], as shown in Eq. 11:

$$\mathbf{h}(t) = \Phi^{\mathrm{T}}\mathbf{M}^{-1}\mathbf{f}_{NL}(t) \tag{11a}$$

or

$$\mathbf{h}(t) = \Phi^{\mathrm{T}}\mathbf{r}(t) \tag{11b}$$

where Φ is the eigenvector matrix associated with the linearized system matrix $\mathbf{M}^{-1}\mathbf{K}$. In this equation, $\mathbf{h}(t)$ represents either the transformed nonlinear residual or transformed nonlinear restoring force, depending on the chosen identification technique.

It may be generally assumed that, in either case, $\mathbf{h}(t)$ will depend on the system's velocity and displacement vectors, as shown in Eq. 12:

$$\mathbf{h}(t) = \mathbf{h}(\mathbf{x}, \dot{\mathbf{x}}) \tag{12}$$

Based on the work established in [42], it may be assumed that each component of $\mathbf{h}$ may be expressed in terms of a series of the form shown in Eq. 13:

$$h_i(\mathbf{x}, \dot{\mathbf{x}}) \approx \sum_{j=1}^{J_{max_i}} \hat{h}_i^{(j)}\left(v_{1_i}^{(j)}, v_{2_i}^{(j)}\right) \tag{13}$$

where v_1 and v_2 are suitable generalized coordinates related, via linear combination, to the physical displacements and velocities. The term J_{max_i} denotes the number of terms needed for a given h_i, and $\hat{h}_i^{(j)}$ refers to the jth modal contribution to the restoring force at the ith DOF. The essence of Eq. 13 is that each component h_i of the transformed nonlinear vector $\mathbf{h}$ may be adequately estimated by a collection of terms $\hat{h}_i^{(j)}$ evaluated at a pair of generalized coordinates. The selection of appropriate generalized coordinates and the number of terms needed to properly estimate h_i depends on the nonlinear characteristics of the system.

Given the distributed nature of the nonlinearities in this (and in a real, physical) MDOF system, an improved rate of convergence of the series in Eq. 13 may be achieved by performing a least squares fit of the nonlinear component (residual or restoring forces) in the "modal" domain. The eigenvector Φ, found previously using the linearized system matrices, may be applied to the displacement vector in the familiar dynamics equation:

$$\mathbf{u}(t) = \Phi^{-1}\mathbf{x}(t) \tag{14}$$

where $\mathbf{u}(t)$ represents the generalized modal displacements of the system. This set of generalized modal coordinates may then be utilized through series of substitutions to yield Eqs. 15a and 15b:

$$\mathbf{h}(\mathbf{u}, \dot{\mathbf{u}}) = \Phi^{\mathrm{T}}\mathbf{M}^{-1}\mathbf{f}_{NL}(t) \tag{15a}$$

or

$$\mathbf{h}(\mathbf{u}, \dot{\mathbf{u}}) = \Phi^{\mathrm{T}}\mathbf{r}(t) \tag{15b}$$

The individual terms contained within the series expansion in Eq. 13 may be evaluated using the least squares approach alluded to earlier. This approach will produce the optimum fit for the time history of each h_i. Equation 16 shows that each $\hat{h}_i^{(j)}$ may therefore be expressed as a double series of a set of generalized modal coordinates q_1 and q_2:

$$\hat{h}_i^{(j)}\left(q_{1_i}^{(j)}, q_{2_i}^{(j)}\right) \equiv \sum_{k}^{k_{\max}} \sum_{l}^{l_{\max}} C_{kl}^{(i)} T_k\left(q_{1_i}^{(j)}\right) T_l\left(q_{2_i}^{(j)}\right) \tag{16}$$

where C_{kl} are the undetermined constants and $T_k(\cdot)$ are suitable basis functions. Once identified, the function representation of each h_i may then be inserted back into the governing equations of motion. A more detailed review of this method, including example applications, may be found in [43,44].

This study will consider two different types of basis functions, a power series basis and Chebyshev poly-

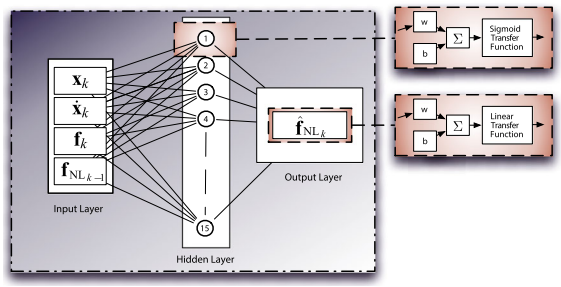

Fig. 2 Schematic for nonlinear residual ANN architecture (adapted from [16])

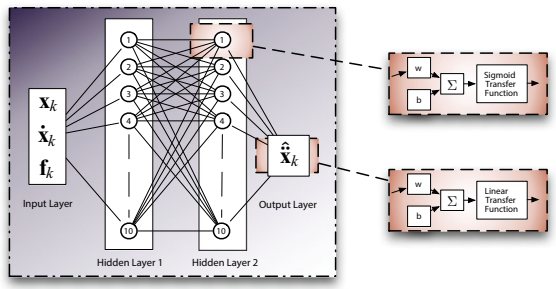

Fig. 3 Schematic for global ANN architecture (adapted from [15])

nomials, as both have been previously used in similar applications [41,42,46]. The power series basis will be applied for both the case of estimating the nonlinear residual and the nonlinear restoring force. The Chebyshev polynomials will only be applied to estimating the nonlinear restoring force, where a Chebyshev polynomial is defined in Eq. 17:

$$T_k(\xi) = \cos(k \cos^{-1} \xi) \qquad -1 \leq \xi \leq 1 \tag{17}$$

Further discussion on the use of Chebyshev polynomials for estimating restoring forces may be found in [42].

2.3 Artificial neural networks

Two different artificial neural networks (ANN) architectures for characterizing nonlinear dynamic systems were explored in the present study [15,16]. A schematic of the first ANN architecture is given in Fig. 2, showing that there is a single input layer, one hidden layer, and a single output layer. A sigmoid transfer function is used for the hidden layer, whereas a linear transfer function is employed in the output layer.

The inputs for the ANN are the displacements $\mathbf{x}_k$, velocities $\dot{\mathbf{x}}_k$, and external excitations $\mathbf{f}_k$ at time t_k for all available DOFs. The nonlinear residual $\mathbf{f}_{NL}$, as determined from Eq. 9, is also included as an input, but this architecture uses a delayed residual from the previous time step t_{k-1}. This is done to enhance the training process and better capture the nonlinear characteristics of the system [16]. The output of the neural network is an estimate of the nonlinear residual at the current time step $\hat{\mathbf{f}}_{NL_k}$. The ANN functions similarly to the polynomial methods described above in that the accelerations at time step t_k will be predicted using a combination of the linear system matrices and the ANN representation of the nonlinear residual.

Figure 3 presents a diagram of the second ANN architecture that suggests a global approach in which the ANN represents the entire system [15]. In this way, the global approach operates in a very similar manner to the VWNN. This architecture includes single input and output layers with two hidden layers in between them. Both hidden layers utilize sigmoid transfer functions, and a linear transfer function is used for the output layer.

Unlike the previously described ANN, this architecture does not include the nonlinear residuals in either its inputs or outputs. As before, the inputs are the displacements, velocities and external excitations from all available DOFs. The outputs in this case are the accelerations of the available DOFs at the current time step $\hat{\ddot{\mathbf{x}}}_k$. One of the advantages of this method is that it does not rely upon a linearization of the system, but rather attempts to fully capture both the linear and nonlinear dynamics of the system.

A substructure ANN architecture is also suggested within [15] in which a different neural network is trained for each DOF using inputs from that DOF and its neighbors. While this method was shown to be highly effective in identifying and estimating nonlinear behavior in a certain class of systems, this method cannot be applied for the case of a generalized topology. The substructure approach requires chain-like structures, or systems that can be easily deconstructed into their constituent DOFs. For the case of a generalized topology in which all DOFs may share some interconnection, however, this is not possible. Therefore only the global ANN approach was included in this study as it shares the same applicability to generalized topologies as the VWNN.

Both ANNs were created using MATLAB's Neural Network Toolbox [47]. A random scheme initialized the weights and biases. Networks were trained using the batch mode of the Levenberg–Marquardt back propagation algorithm. The performance function was defined in terms of mean squared error.

3 Applications

Each of the different methods under discussion was applied to responses generated by the model structure shown in Fig. 4. The structural topology is such that the model is composed of three masses m_i that are interconnected to a system of six restoring force elements r_i that are anchored to a support s_i at three locations. The supports $s_i(t)$ may be fixed or moving. This results in a redundant system with three degrees of freedom. All motion is one-dimensional, as the structure only allows rectilinear horizontal motion. Since the structure is not chain-like, the linearized system stiffness matrix will not be banded.

The absolute displacement of each mass m_i is designated by x_i. The external excitation forces that act upon this system are denoted by $f_i(t)$. The magnitudes of the system masses are $m_1 = 0.8$, $m_2 = 2.0$ and $m_3 = 1.2$, and these remain the same for all simulations.

3.1 Models for nonlinear restoring forces

The restoring force elements r_i are dependent on the relative displacement y_i and velocity $\dot{y}_i$ across the terminals of each element. The relative motions across the various elements $y_i(t)$ are determined as follows:

$$y_1 = x_1 - s_1 \tag{18a}$$
$$y_2 = x_2 - x_1 \tag{18b}$$
$$y_3 = x_3 - x_1 \tag{18c}$$
$$y_4 = x_3 - x_2 \tag{18d}$$
$$y_5 = s_3 - x_3 \tag{18e}$$
$$y_6 = x_2 - s_2 \tag{18f}$$

Each element has prescribed nonlinear behavior. The type of nonlinearity, however, was varied between a few different simulations.

3.1.1 Bilinear hysteresis and limited-slip elements

The restoring force elements were first given bilinear hysteretic and limited-slip behaviors, as shown in Fig. 5; the behavior of these elements are governed by

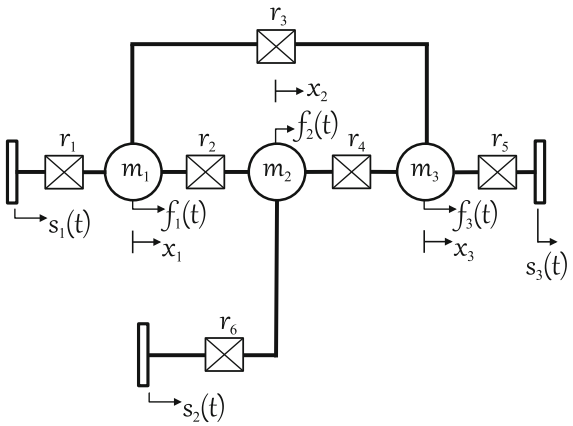

Fig. 4 Model of generic nonlinear 3DOF system

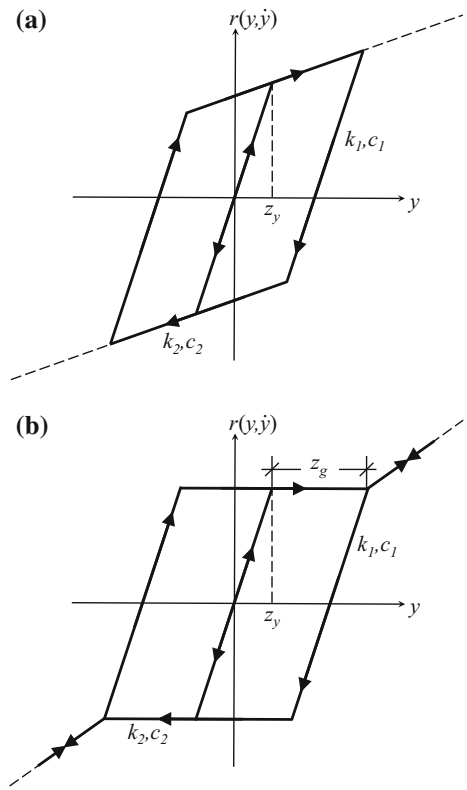

Fig. 5 Sample plots of restoring force versus relative displacement for **a** bilinear hysteretic and **b** limited-slip elements

Table 1 Restoring force element properties for bilinear and limited-slip behaviors

Element i	Type	$p_1^{(i)}$	$p_2^{(i)}$	$p_3^{(i)}$	$p_4^{(i)}$	$p_5^{(i)}$	$p_6^{(i)}$
1, 5, 6	Bilinear	$z_y = 0.02$	$k_1 = \mathrm{k_0}$	$k_2 = 0.5\mathrm{k_0}$	$c_1 = 0.01$	$c_2 = 0.01$	–
2, 3, 4	Limited-slip	$z_y = 0.01$	$k_1 = \mathrm{k_0}$	$k_2 = \mathrm{k_0}$	$c_1 = 0.1\mathrm{c_0}$	$c_2 = 0.1\mathrm{c_0}$	$z_g = 0.03$

the branches and trajectories shown via arrows in Fig. 5. Following the example in [46], elements r_1, r_5, and r_6 were designated as bilinear hysteretic, while the other three elements (r_2, r_3, and r_4) were of the limited-slip type. For the bilinear elements, five element parameters must be specified: the stiffness and viscous damping in the elastic range k_1 and c_1, respectively, the stiffness and viscous damping in the nonlinear range k_2 and c_2, respectively, and the yield displacement level z_y. The limited-slip elements include a sixth term, the slip displacement level z_g. The material properties and specific parameter values chosen for this study were taken directly from [46] and are shown in Table 1. The nominal stiffness in the elastic range $\mathrm{k_0}$ is set at $4\pi^2$ for all elements, and the nominal damping coefficient $\mathrm{c_0}$ is set at $\pi/4$.

Phase-plane plots of the bilinear hysteretic and limited-slip restoring forces from a sample simulation are shown in Fig. 6. The bilinear behavior of elements r_1, r_5 and r_6 and the limited-slip behavior of elements r_2, r_3 and r_4 may be clearly observed.

3.1.2 Polynomial nonlinearity

The restoring force elements were then changed to exhibit polynomial nonlinearities. The nonlinearity for each element was expressed using Eq. 19, where $p_1^{(i)}$ represents the linear stiffness component, $p_2^{(i)}$ represents the linear viscous damping term and $p_3^{(i)}$ is the coefficient for the cubic (nonlinear) displacement term. By changing the sign of $p_3^{(i)}$ the restoring force element r_i will either represent hardening (positive) or softening (negative) nonlinear behavior.

$$r_i(y, \dot{y}) = p_1^{(i)} y_i + p_2^{(i)} \dot{y}_i + p_3^{(i)} y_i^3 \tag{19}$$

The specific nonlinear element properties were adopted from the example in [41] that keeps the nominal stiffness of all elements at $p_1^{(i)} = 4\pi^2$. The viscous damping was defined as $p_2^{(i)} = \pi/5$, and the cubic displacement terms were proportional as $p_3^{(i)} = \pm 0.5 p_1^{(i)}$, where $i = 1, 5$ and 6 are positive (+) and $i = 2, 3$ and 4 are negative (−). A sample of the phase-plane restoring force plots generated by the cubic nonlinearities are shown in Fig. 7. As with the previous example, the material properties were varied to evince two different types of polynomial nonlinear behavior: hardening (r_1, r_5 and r_6) and softening (r_2, r_3 and r_4).

3.1.3 Bouc–Wen hysteresis

Simulations were also conducted in which the restoring forces were governed by a Bouc–Wen model for hysteresis [5,6], shown in Eq. 20:

$$\dot{r}_i = (1/\eta_i)\left[A_i \dot{y} - \nu_i \left(\beta_i \, |\dot{y}| \, |r_i|^{n_i - 1} \, r_i - \gamma_i \dot{y} \, |r_i|^{n_i}\right)\right] \tag{20}$$

where η_i, A_i, ν_i, β_i, γ_i, and n_i are design parameters for the hysteretic behavior. In order to reduce the number of terms in Eq. 20, the parameters η_i and ν_i, which are typically used to control degrading and pinching behavior [60], respectively, were uniformly set to unity for all restoring force elements. Additionally, the parameter n_i was consistently set to unity for each restoring force element.

The Bouc–Wen parameter related to linear stiffness, A_i, was set as the same nominal stiffness ($4\pi^2$) used for the other two nonlinear models. The remaining parameters were set as ratios of A_i, namely $\beta_i = A_i/4$ and $|\gamma_i| = A_i/3$. (It should be noted that the thermodynamic principle of intrinsic dissipation would typically require $|\gamma| \leq \beta$ [18], but this particular constraint is not of concern for the current example.) The same parameters were given to every element, but the sign of γ_i was positive for $i = 1, 5$, and 6 and negative for $i = 2, 3$, and 4. These parameter choices and ratios were influenced by the Bouc–Wen hysteresis loops produced by SDOF system shown in [53].

Figure 8 shows the hysteresis loops produced by the Bouc–Wen restoring force elements. The influence of the sign of γ_i may be clearly seen when comparing elements, as it allows for both hardening and softening

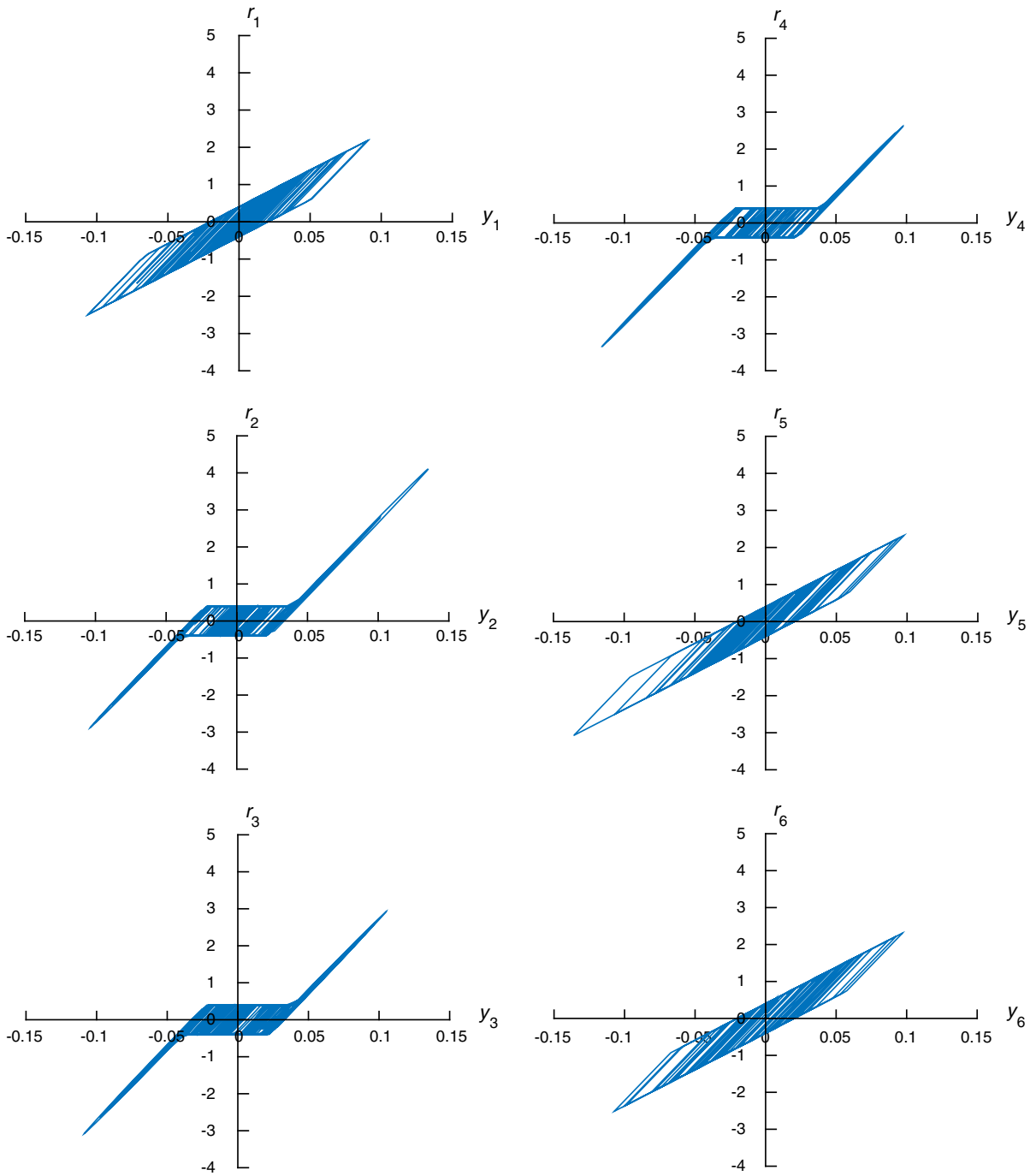

Fig. 6 Phase-plane plots (restoring force vs. relative displacement across element) of the bilinear hysteretic (r_1, r_5 and r_6) and limited-slip (r_2, r_3 and r_4) nonlinear elements. Note that identical scales were used for all of the plots

behaviors. Additionally, these phase-plane plots show that the restoring force elements experienced fairly significant hysteresis with Bouc–Wen models, as each plot shows significant drift among the many loops. It was assumed that such extensive hysteresis would prove challenging during identification, but the extent

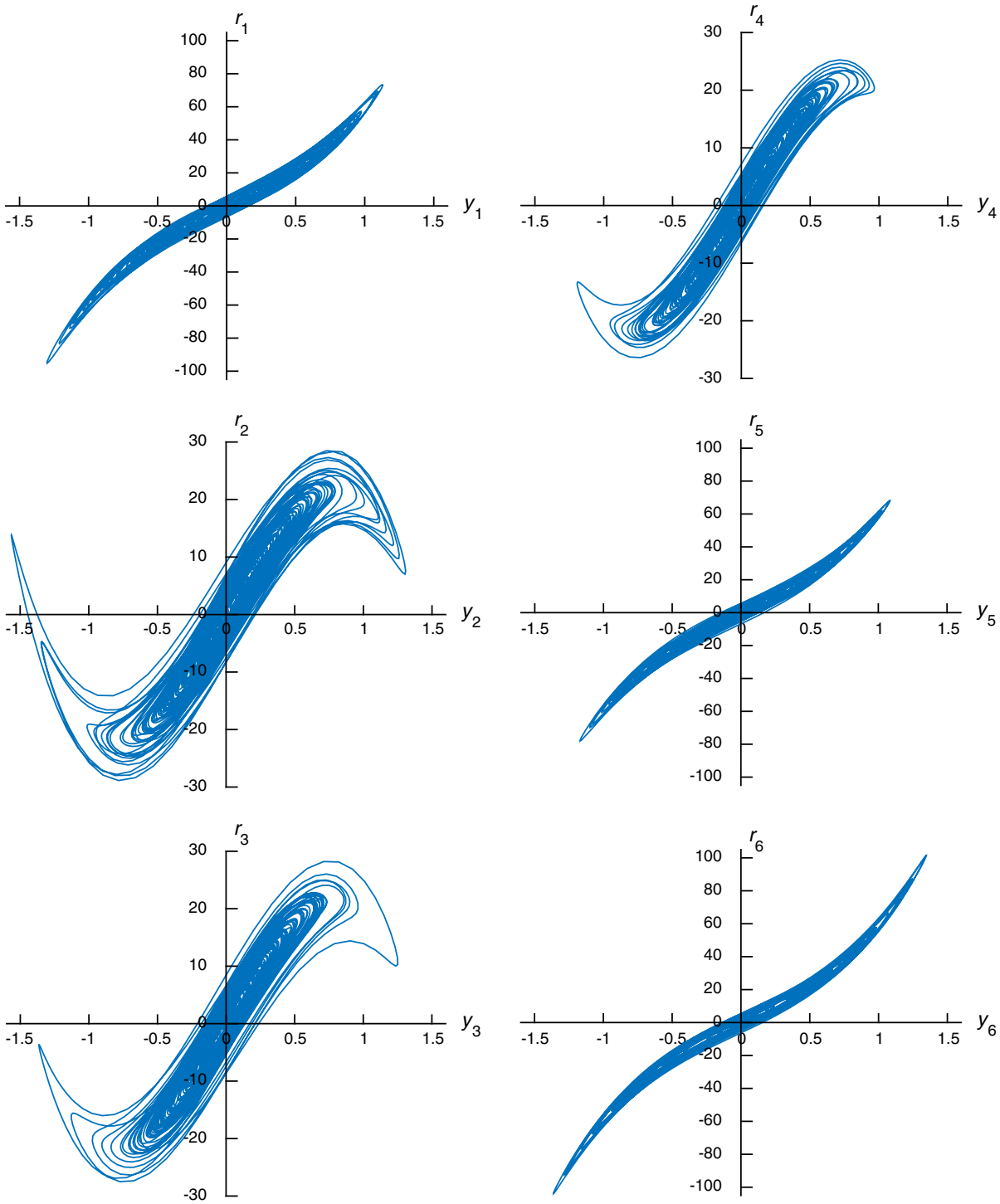

Fig. 7 Phase-plane plots (restoring force vs. relative displacement across element) of the hardening (r_1, r_5 and r_6) and softening (r_2, r_3 and r_4) nonlinear elements. To enhance visualization, different amplitude scales were used for the individual plots of the hardening and softening elements

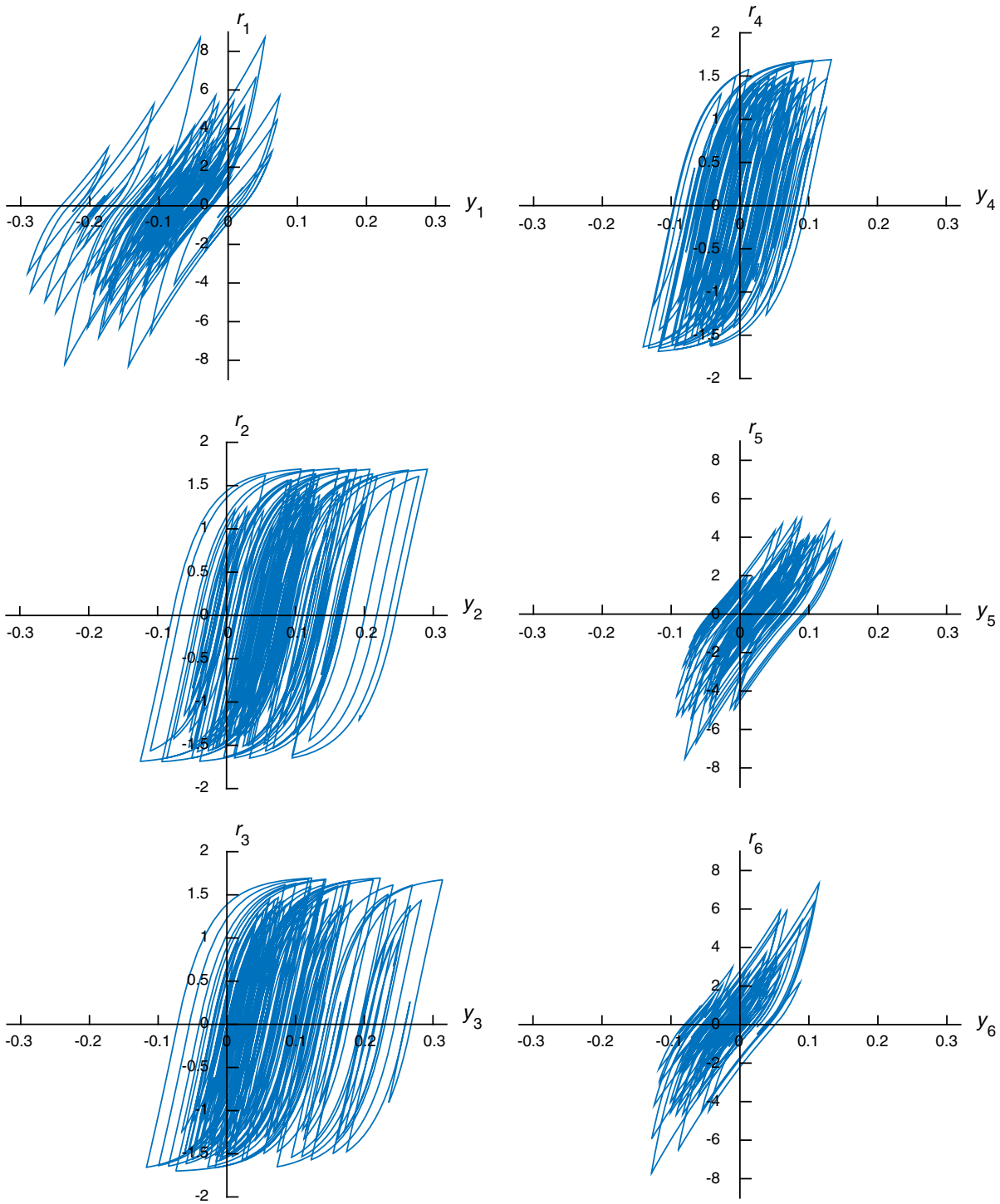

Fig. 8 Phase-plane plots (restoring force vs. relative displacement across element) of the Bouc–Wen hysteretic elements. To enhance visualization, different amplitude scales were used for the individual plots

of the challenge was unknown prior to attempting each method.

3.2 Training and testing

The different identification methods explored for this study do not impose restrictions on the nature of the excitation sources. Therefore, excitation $\mathbf{f}(t)$ was provided by uncorrelated broad-band random excitations applied to each of the three system masses. The random excitations were modeled as zero-mean stationary random processes, with the standard deviations varying between restoring force models in order to elicit a wide range of nonlinear behaviors from each model. The random excitations were also relatively broad-band in nature in order to fully excite the dynamics of the 3DOF system. The duration of each simulation was 50 s in order to allow for at least 50 periods of the fundamental frequency for each system.

Two types of simulations were conducted for each system: a training simulation and subsequent test simulation, where each simulation followed the general procedure described above and was used to produce the measurements, *i.e.*, the excitations and responses, used for evaluating the nonlinear identification methods; for both types of simulations, full state information and excitations were provided to each method. Thus, the displacements, velocities and accelerations, as well as the external excitations from each DOF, were made available; however, while all of these quantities were available, their use or incorporation depended on the desired inputs of a given method. This allowed each method to produce its optimal fit as the focus of this paper is the nonlinear identification capabilities of the different methods.

First a training simulation was used for fitting the relevant coefficients or training the specified networks depending on the given method. The performance of each method in identifying the nonlinear system was quantified based on the ability to estimate the original measured accelerations. The accuracy of the estimates was evaluated using the relative root-mean-square (RMS) error, as calculated in Eq. 21, which takes the acceleration responses from all three DOFs into account. In Eq. 21, $\ddot{\mathbf{x}}$ represents the measured accelerations and $\hat{\ddot{\mathbf{x}}}$ represents the estimate of the accelerations as produced by a given method. This relative RMS error will serve as the primary performance metric.

$$RMS\,(t_n) = \frac{\sqrt{\sum_{i=1}^{n}\left(\ddot{\mathbf{x}}(t_i)-\hat{\ddot{\mathbf{x}}}(t_i)\right)^{\mathrm{T}}\left(\ddot{\mathbf{x}}(t_i)-\hat{\ddot{\mathbf{x}}}(t_i)\right)}}{\sqrt{\sum_{i=1}^{n}\left(\ddot{\mathbf{x}}(t_i)\right)^{\mathrm{T}}\ddot{\mathbf{x}}(t_i)}} = \frac{\|\hat{\ddot{\mathbf{x}}}-\ddot{\mathbf{x}}\|}{\|\ddot{\mathbf{x}}\|} \tag{21}$$

The error from training represents the "fit" error for a given method, as there is no forward computational simulation aspect and, therefore, no "propagation" error source.

For the test simulations, the 3DOF system was subjected to a new set of random excitations with the same spectral characteristics. These new system responses and excitations were then fed directly into each method, again avoiding the need for forward computational simulation within a given method. The estimated accelerations from the test simulations were determined using the coefficients or weights produced during training. For instance, for the polynomial identification methods, the previously determined equivalent linear system matrices were used to estimate the linear acceleration responses given the new displacements, velocities, and excitations; the new generalized displacements and velocities were used as inputs for the previously created nonlinear polynomial function. When combined, they would create an estimate for the acceleration responses from the test simulation based on the matrices and coefficients identified during training (fitting); a similar procedure was followed for the VWNN and ANN methods. The same relative RMS error was used to evaluate the estimated accelerations.

3.3 Parameters for nonlinear identification techniques

Each method includes a few parameters that must be specified by the user prior to implementation. In an effort to create fair comparisons between methods, and between nonlinear behaviors, parameters were kept constant where possible.

3.3.1 Volterra/Wiener neural network

The main parameters that must be specified for the VWNN are shown in Table 2. For the low-pass filter in the first row, the cut-off frequency is given as 50 rad/s, which is well above any of the frequencies in the responses created by the various nonlinear elements. The second row denotes the number of low-

Table 2 Parameters for Volterra/Wiener neural network

$H(s)$	$50/(s+50)$
No. cascading filters	2
$W^{\mathrm{T}}\phi(\xi)$	Second-order HONN

pass filters applied in cascade to the original input. The third row denotes that the HONN for each system was chosen to be second-order. The only parameter not included in Table 2 is the weight from the hyperbolic tangent sigmoidal function λ. This parameter is related to the input, and was therefore scaled based on the input accelerations and excitations. The bilinear and Bouc–Wen hysteretic simulations produced accelerations with a range around ± 10, but the polynomial nonlinearity simulation produced accelerations around ± 100. Therefore, λ was set at 0.05 for the bilinear and Bouc–Wen simulations and 0.005 for the polynomial nonlinearity simulations.

3.3.2 Polynomial basis methods

The order of the power series basis was set at $j_{max} = 5$ for the functions estimating both the nonlinear residuals and nonlinear restoring forces. Equation 22 shows the corresponding power series basis of length 36:

$$\begin{aligned}\text{basis} = \{&1, q, q^2, q^3, q^4, q^5, q\dot{q}, q^2\dot{q}, q^3\dot{q},\\ &q^4\dot{q}, q^5\dot{q}, q\dot{q}^2, q^2\dot{q}^2,\\ &q^3\dot{q}^2, q^4\dot{q}^2, q^5\dot{q}^2, q\dot{q}^3,\\ &q^2\dot{q}^3, q^3\dot{q}^3, q^4\dot{q}^3, q^5\dot{q}^3, q\dot{q}^4,\\ &q^2\dot{q}^4, q^3\dot{q}^4, q^4\dot{q}^4, q^5\dot{q}^4,\\ &q\dot{q}^5, q^2\dot{q}^5, q^3\dot{q}^5, q^4\dot{q}^5, q^5\dot{q}^5\}\end{aligned} \tag{22}$$

The same basis was used in order to provide unbiased comparisons in performance since no prior knowledge was assumed for any of the nonlinear parameters or characteristics.

Similar to the scaling of inputs performed for the VWNN, the generalized coordinates were normalized prior to using least squares to solve for the coefficients. The normalization is performed using Eqs. 23a and 23b:

$$q' = [q - (q_{\max} + q_{\min})/2]/[(q_{\max} - q_{\min})/2] \tag{23a}$$

$$\dot{q}' = [\dot{q} - (\dot{q}_{\max} + \dot{q}_{\min})/2]/[(\dot{q}_{\max} - \dot{q}_{\min})/2] \tag{23b}$$

The normalization prevents the terms with higher-degree polynomials from "blowing up," providing some stability to the power series expression. However, it is important to note that the normalization is performed with regard to the responses from *training* and without any knowledge of the response amplitudes from the test simulation. Therefore, it is possible for response amplitudes from the test simulation to exceed those from training and, consequently, for terms in the basis to exceed ± 1 during testing. The potentially deleterious effects of these exceedances, though, should be significantly mitigated by the normalization.

Similar to the power series, the Chebyshev polynomial basis was fifth-order for both generalized coordinates and produced a total of 36 coefficients. Additionally, the coordinates were normalized according to Eqs. 23a and 23b, as Chebyshev polynomials are defined for an input range of ± 1.

3.3.3 Artificial neural networks

The ANN used to estimate the nonlinear residual had a total of 12 inputs (three displacements, three velocities, three external excitations, and three delayed nonlinear residuals). Based on the work in [16], this ANN was given a hidden layer of 15 hidden neurons. The transfer function for the hidden layer was prescribed as a hyperbolic tangent sigmoid transfer function. This was based on recommendations in [16] but also made for a suitable comparison to the VWNN. The ANN produced three outputs (nonlinear residuals).

The ANN for the global approach had only nine inputs (three displacements, three velocities, and three external excitations). Each of its two hidden layers contained ten hidden neurons and used hyperbolic tangent

Table 3 Relative RMS errors from various identification strategies for the bilinear nonlinear model

ID method	Total RMS error (in %)	
	Training	Testing
VWNN	9.34	10.79
PS—residual	19.32	36.24
PS—restoring force	19.78	19.60
Ch—restoring force	19.73	19.55
ANN—residual	2.40	42.25
ANN—global	15.43	22.17

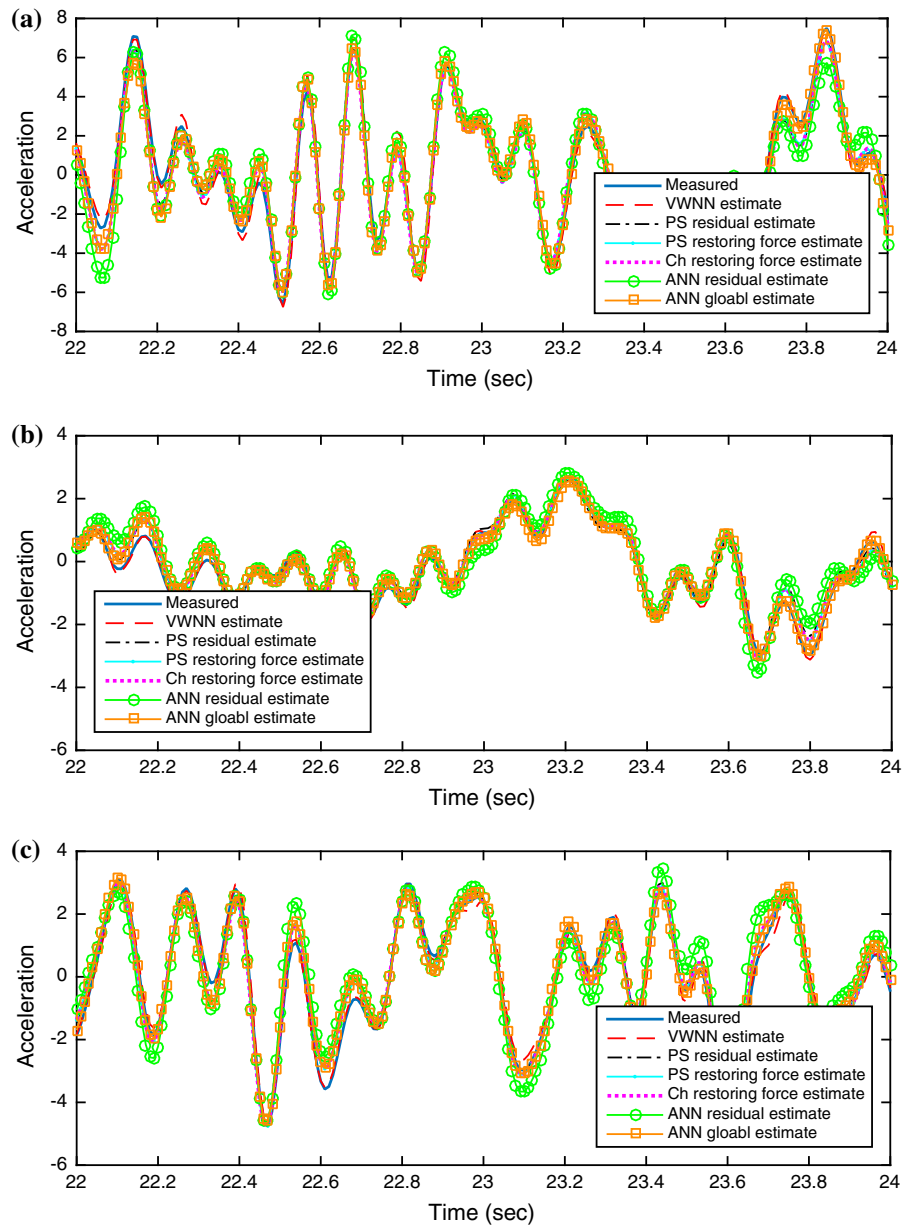

Fig. 9 Comparison of exact and estimated accelerations for the **a** 1st, **b** 2nd, and **c** 3rd DOFs from the test simulation conducted using bilinear nonlinear models

sigmoid transfer functions. Three outputs (accelerations) were produced. The design of this ANN was based on recommendations in [15].

While the authors recognize that the number of hidden layers and the number of neurons could potentially be adjusted to further optimize the system, similar changes and adjustments could also be made to other methods to further optimize their results. Therefore, the authors thought it was best to design these ANN architectures according to the established designs in [15,16] given the similarity in application.

4 Results and discussion

The bilinear hysteresis simulations were conducted first. The relative RMS errors for the estimated accelerations produced by each of the nonlinear identifica-

tion techniques are shown in Table 3, where "PS—residual" and "PS—restoring force" refer to estimates found using power series polynomial estimates for the nonlinear residuals and restoring forces, respectively, and "Ch—restoring force" refers to estimates found using Chebyshev polynomial functions for the restoring forces. The first column displays the results from training, during which the various neural networks and polynomial functions were assembled and estimated, and the second column represents the performance of these methods given a new excitation and new state information, *i.e.*, different accelerations, velocities and displacements, for testing.

The polynomial methods (both power series approaches and the Chebyshev technique) produced generally comparable estimates for both the training and test simulations. While the ANN residual-based method produced the most accurate representation of the accelerations during training, it also produced the least accurate estimate during testing. The VWNN was relatively accurate during training and the RMS error in its test simulation estimate was comparable and nearly 50 % smaller than all other estimates.

As mentioned previously, the ANNs were created using the MATLAB Neural Network Toolbox [47] that employs random seeds for training the network. Because of this feature, the results from an ANN would be slightly different each time it is run. The results in Table 3 (and all subsequent tables) are from single trials for the ANN approaches, but those results may be considered representative, as a few trials were run in order to ensure a general congruency in the RMS errors. The other methods, including the VWNN, are deterministic in nature. In terms of training, the ANN residual approach required around 150 epochs to satisfy the prescribed performance criteria, whereas the global ANN approach required around 240 epochs.

Figure 9 shows the estimated accelerations from the test simulation at each DOF produced by the different identification methods and plotted over a relatively small time window (a smaller time window was necessary to provide discernible differences between the methods). Subtle differences in the estimates may be detected, but generally the methods provided fairly similar estimates of the measured accelerations.

The results of the polynomial nonlinearity simulation are given in Table 4. Much like the previous results, the power series and Chebyshev polynomials produced comparable estimates, and these were more accurate than they were for the bilinear hysteretic case. During training, both ANN approaches (residual and global) failed to achieve their performance criteria prior to 1000 epochs; however, both ANN approaches were nearly perfectly accurate in their estimation of the training simulation. Only the global ANN performed comparably during testing. The VWNN was not as accurate as the global ANN but proved to be reasonably accurate during both the training and testing simulations.

Table 4 Relative RMS errors from various identification strategies for the polynomial nonlinear model

ID method	Total RMS error (in %)	
	Training	Testing
VWNN	3.43	4.71
PS—residual	11.87	11.13
PS—restoring force	13.16	11.27
Ch—restoring force	12.68	11.01
ANN—residual	0.10	8.94
ANN—global	0.12	0.26

The estimated accelerations for the test simulation shown in Fig. 10 are essentially indistinguishable between methods, which reflects the consistent accuracy and low errors given in Table 4.

The Bouc–Wen simulations proved to be the most difficult case for identification for all of the methods except the VWNN. The RMS errors for the VWNN were remarkably similar to the polynomial nonlinear model case, but every other method experienced a significant increase in error during training and an order-of-magnitude increase for the test simulation (Table 5). Among those affected, the residual ANN approach had the best estimate (by far) for the training simulation, but its results for the test simulation were as poor, or worse, than every other method. The residual ANN approach required about 400 epochs during its training, whereas the global ANN approach only required around 80 epochs. Despite this disparity during training, they performed comparably poorly for the test simulation.

The sharp rise in RMS error was not entirely a surprise given the intense drift and numerous hysteresis loops shown by the Bouc–Wen phase-plane plots in Fig. 8. However, more insight may be gained by exploring the acceleration estimates. The estimated accelerations produced by the different identification meth-

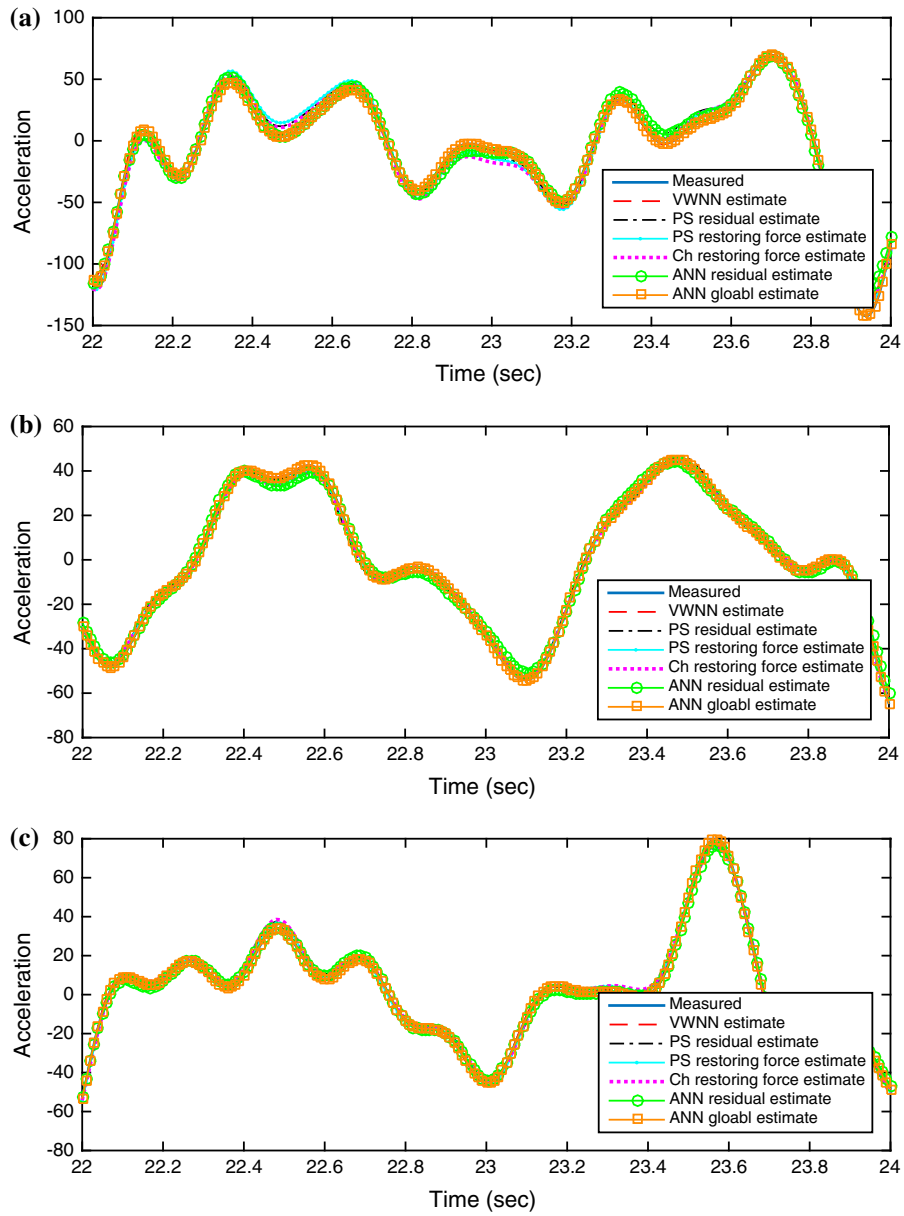

Fig. 10 Comparison of exact and estimated accelerations for the **a** 1st, **b** 2nd, and **c** 3rd DOFs from the test simulation conducted using polynomial nonlinear models

ods for the test simulation are plotted in Fig. 11. This figure demonstrates that the VWNN method follows the measured acceleration very closely (the two superimposed curves are virtually indistinguishable) and that the polynomial-based identification methods follow similar trajectories, albeit trajectories that are relatively in-phase but at a significant off-set from the measured accelerations. Even the different ANN techniques seem to capture some of the larger dynamics of the system, but their off-sets and phase shifts are less consistent. More importantly, Fig. 11 also shows that the two ANN approaches produced very different estimates even though they produced roughly the same total RMS error. There were general estimation errors for each method, in addition to the phase shifts and off-sets, but those more demonstrable features clearly contributed to the errors being in excess of 100 %.

Table 6 presents the relative RMS errors for each individual DOF, essentially providing a breakdown of the RMS errors in Table 5. From this table it may be observed that during the training simulation all of the DOFs were generally estimated with the same degree

Table 5 Relative RMS errors from various identification strategies for the Bouc–Wen hysteretic nonlinear model

ID method	Total RMS error (in %)	
	Training	Testing
VWNN	3.64	5.31
PS—residual	64.63	157.26
PS—restoring force	64.07	115.90
Ch—restoring force	64.13	116.69
ANN—residual	1.07	170.08
ANN—global	44.86	172.37

of accuracy for each individual method under discussion. However, this table also shows that during testing all of the polynomial identification methods struggled with estimating the accelerations for the 2nd and 3rd DOF much more than for the 1st DOF. Further, it shows that the global ANN method produced a more reasonable estimate for the 2nd DOF, even though its error from the estimate for the 1st DOF approached 200 %. The residual ANN approach produced its best estimate for the 2nd DOF and its worst for the 3rd DOF. Clearly, none of the DOFs were universally favored by the different identification methods during testing but each method seemed to find a particular DOF (or two) with which it especially struggled.

4.1 Incomplete response information

The results shown above assumed that all of the response information, including displacements and velocities, would be available for measurement at every DOF. While this assumption helps each method to produce the best possible estimates, it does not represent the most realistic scenario. More commonly, only accelerations are available for measurement and the velocity and displacement information must be obtained through numerical integration [16,49]. To properly integrate numerically, a series of high-pass filters must be used before and after each integration step. This helps reduce drift caused by low frequency errors but does not eliminate it, meaning the resulting numerical velocity and displacements will still contain some degree of unavoidable error.

This poses a significant disadvantage for all methods, except the VWNN, as they all rely upon this additional response information. The error introduced during integration will propagate through the estimation process. In order to determine the potential impact of numerical integration effects on these different identification methods, the measured displacement and velocity responses were removed from the training and test simulations for the polynomial nonlinear model and these response quantities were replaced by their corresponding numerical integrals. The polynomial simulation was chosen because the different methods produced their most accurate estimates for this nonlinear system model, and therefore the effect of numerical integration could be most readily observed.

The relative RMS errors in the estimates under such conditions are given in Table 7. For the different polynomial-based methods, the numerical integration of the acceleration resulted in a 20–25 % relative increase in the relative RMS error. However, the ANN methods were considerably more sensitive. The ANN residual-based method had a minimal increase in error during training, but its estimate for the test simulation had an order-of-magnitude larger error than it had previously. The global ANN approach experienced a large increase in error, too. However, this increase was present for both the training and test simulation results. The results serve to highlight the strength of the VWNN's identification abilities, since it only relies upon the acceleration and external excitations.

4.2 Measurement noise

As opposed to incomplete information about the responses, another possible scenario is that the sensors being used to record the system responses all contain some amount of noise. In order to replicate such a scenario, noise was added to the response data (displacements, velocities, and accelerations) from the polynomial nonlinear model simulations. (As a clarification, the datasets used were from the original simulation scenario in which all of the responses, including displacements and velocities, were measured and available). The noise was modeled as additive Gaussian white noise with zero-mean and standard deviations that had ratios of 10 % of their related response quantity, meaning the signal-to-noise ratio was 10. No noise was added to the excitation data.

The resulting RMS errors from the noisy response data are given in Table 8. The addition of noise seemed

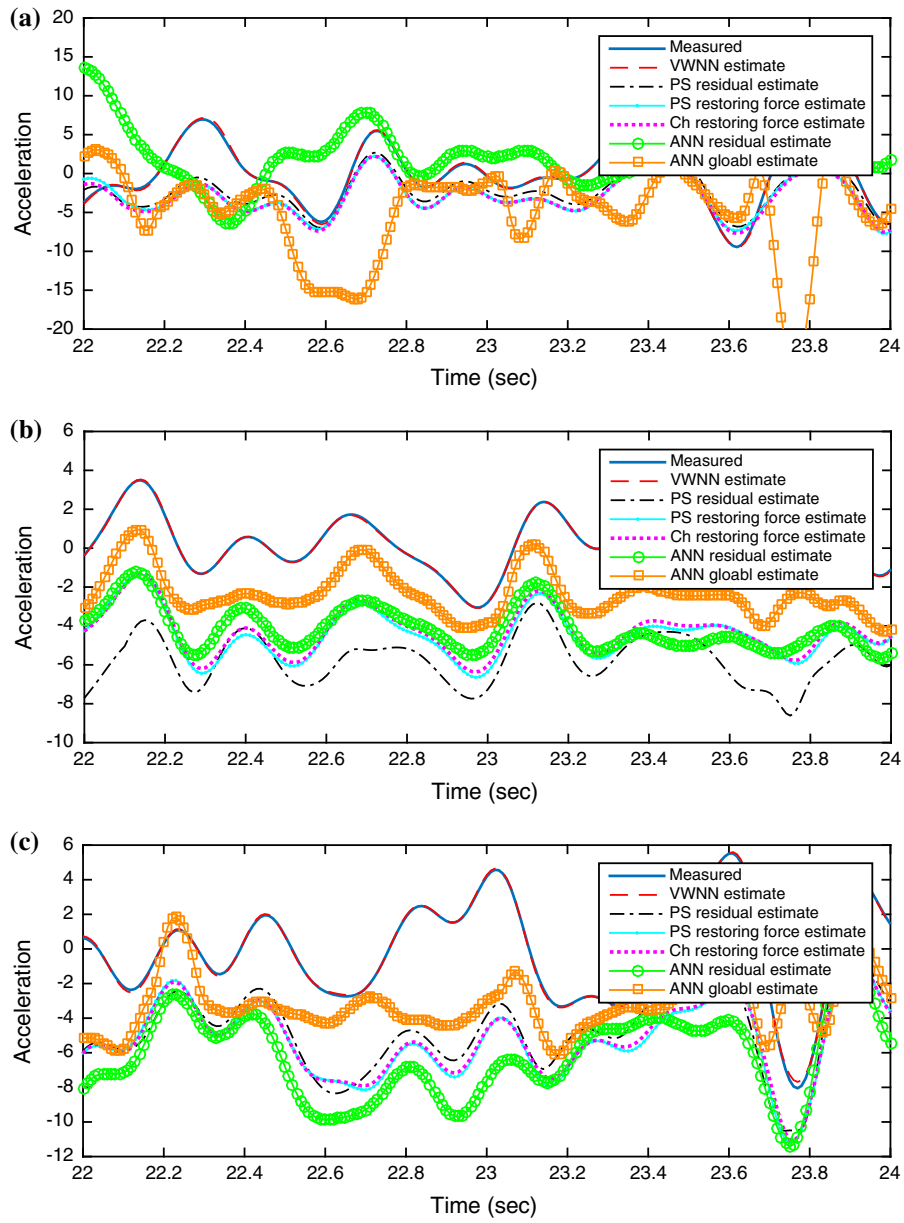

Fig. 11 Comparison of exact and estimated accelerations for the **a** 1st, **b** 2nd, and **c** 3rd DOFs from the test simulation conducted using Bouc–Wen nonlinear models

Table 6 Relative RMS errors (in %) at each DOF for the Bouc–Wen hysteretic nonlinear model

ID method	Training			Testing		
	1st DOF	2nd DOF	3rd DOF	1st DOF	2nd DOF	3rd DOF
VWNN	4.26	1.47	2.26	6.23	2.11	3.42
PS—residual	67.38	73.59	53.26	95.13	256.59	216.60
PS—restoring force	67.90	57.09	56.06	91.45	155.75	146.75
Ch—restoring force	67.99	56.45	56.30	91.93	156.69	148.01
ANN—residual	1.04	1.30	1.05	155.71	151.16	206.01
ANN—global	43.87	47.83	46.19	199.10	85.50	119.56

Table 7 Relative RMS errors from various identification strategies for the polynomial nonlinear model using numerically integrated response information

ID method	Total RMS error (in %)	
	Training	Testing
VWNN	3.43	4.71
PS—residual	15.24	13.25
PS—restoring force	16.21	14.29
Ch—restoring force	15.22	13.26
ANN—residual	0.65	33.07
ANN—global	8.37	9.98

Table 8 Relative RMS errors from various identification strategies for the polynomial nonlinear model with sensor noise included in the measured responses

ID method	Total RMS error (in %)	
	Training	Testing
VWNN	13.13	13.63
PS—residual	22.14	20.07
PS—restoring force	22.64	20.33
Ch—restoring force	22.18	20.07
ANN—residual	10.47	18.94
ANN—global	18.90	18.31

to lead to a near uniform 10 % increase in the RMS error as compared to the estimates in Table 4. Only the global ANN approach suffered a more drastic increase as its RMS error went from near zero to 18 % with the addition of the noise. The RMS error from polynomial-based methods responded similarly for the introduction of error via numerical integration, but since the error was now present in all of the response data, the total RMS error was larger than in Table 7 but still generally proportional. Unlike the case for the numerically integrated responses, the VWNN method was compromised by the addition of measurement noise and saw its error increase 10 % (from 3–4 to 13 %). However, the more significant increase to the global ANN approach meant that the VWNN provided the best results.

4.3 Parameter adjustments

It is possible that some of these methods could produce better results if parameters were carefully adjusted or tuned. For power series basis methods, different orders could be investigated and used for each type of nonlinearity. For the Chebyshev polynomials the assumed order of the generalized coordinates are independent, and therefore several possible combinations could be evaluated in hopes of finding on optimal basis order for each nonlinear model. Perhaps most obviously, the ANN architectures could be slightly modified to include slightly fewer or slightly more hidden neurons or hidden layers. However, even the VWNN had its own set of parameters with which experiments could have been designed in order to fully realize its estimation potential.

The authors took all of this into consideration prior to running these simulations but felt that the main purpose of this study was to determine the effectiveness of a general set of parameters for a given identification method, when applied to a variety of nonlinear models. The results, especially those for the Bouc–Wen nonlinear models, indicate that these methods have room for improvement in terms of their parameters. However, their overall performance for the other nonlinear models was generally consistent and reasonably accurate, substantiating the claim that the present study provided its intended "fair" comparison.

5 Conclusions

The variety of nonlinear models considered for the restoring forces of the 3DOF system presented a strong set of challenges for the nonlinear identification methods considered. By performing the identification using batch estimation methodologies, each identification technique was given the best opportunity to find its optimal parameters. The case of polynomial nonlinearity proved to be the easiest to accurately approximate with the largest RMS errors at only 12–13 % across all methods. The Bouc–Wen model proved by far the most difficult with every method except the VWNN failing to provide an estimate from testing with RMS errors below 100 %. This was precipitated by the challenging nature of the Bouc–Wen nonlinearities and the large drifts in the hysteresis loops of the Bouc–Wen model restoring forces, as every method but the VWNN relied upon displacement and velocity response information for its estimates.

The introduction of error due to numerical integration of the responses or measurement noise led

to noticeable but small increases in error. Since the VWNN only requires acceleration and excitation information, it was unaffected by the numerical integration error. However, its error rose in correspondence with the other methods when measurement noise was added. The unifying theme through this investigation, though, was the resilience of the VWNN method in nonlinear identification. Across all models and scenarios, the VWN consistently performed well, often the best, and had its error reach a maximum of only 13 % (a modest error, considering the complexity of the investigated nonlinear models). In comparison with other neural network methods, the VWNN displayed much less sensitivity than the ANN approaches, but that was rather expected given how those methods rely upon displacement and velocity information. In some ways the VWNN actually operated more closely to the polynomial methods in that the hyperbolic tangent sigmoid functions served as basis functions, and its optimal linear coefficients could be determined via least squares.

Another advantage of the VWNN method is that it already has a demonstrated its ability to work in an adaptive on-line fashion, which could be quite valuable for control applications. While its possible some of the other methods included in this study could be similarly adapted for on-line identification, none have developed that capability, yet. Even considering the relatively impressive performance of the VWNN method, it is not without its own faults. Many of the other identification methods may also be used for forward simulations and computation, but the VWNN currently lacks that ability. Additionally, even in its current form, the VWNN is best suited for control-based applications as it relies upon measurement information at each time step. It is suggested that future research focus on harvesting the VWNN's identification abilities and transferring them into a forward computational engine in which the VWNN can use its own estimates as opposed to measurements. In addition, this study is in no way meant to be exhaustive as there are a variety of other nonlinear models and topologies in need of further investigation and evaluation for identification purposes.

Acknowledgments The first author would like to acknowledge the support of the Viterbi Postdoctoral Fellowship from the University of Southern California. The assistance of Dr. Armen Derkevorkian in lending his expertise of artificial neural networks and generously granting permission to modify figures from his own works is gratefully acknowledged.

References

1. Andronikou, A., Bekey, G.A.: Identification of hysteretic systems. In: 18th IEE Conference on Decision and Control (1984)
2. Antoni, J.: Blind separation of vibration components: principles and demonstrations. Mech. Syst. Signal Process. **19**, 1166–1180 (2005)
3. Baber, T., Noori, M.: Random vibration of degrading, pinching systems. ASCE J. Eng. Mech. **111**(8), 1010–1026 (1985)
4. Baber, T., Noori, M.: Modeling general hysteresis behavior and random vibration application. J. Vib. Acoust. Stress Reliab. Des. **108**(4), 411–420 (1986)
5. Baber, T., Wen, Y.: Stochastic equivalent linearization for hysteretic, degrading, multistory structures. Technical Report, Civil Engeering Studies, SRS No. 471, University of Illinois, Urbana, Illinois (1979)
6. Baber, T., Wen, Y.: Random vibration of hysteretic degrading systems. J. Eng. Mech. Div. ASCE **107**, 1069–1087 (1981)
7. Benedettini, F., Capecchi, D., Vestroni, F.: Identification of hysteretic oscillators under earthquake loading by nonparametric models. ASCE J. Eng. Mech. **121**, 606–612 (1995)
8. Bouc, R.: Forced vibration of mechanical systems with hysteresis. In: 4th Conference on Nonlinear Oscillation, Prague, Czechoslovakia (1967)
9. Brincker, R., Andersen, P., Zhang, L.: Modal identification from ambient responses using frequency domain decomposition. In: Proceedings of the 18th International Modal Analysis Conference (IMAC), San Antonio, TX, pp. 625–630 (2000)
10. Caughey, T.: Random excitation of a system with bilinear hysteresis. ASME J. Appl. Mech. **27**, 649–652 (1960)
11. Chassiakos, A., Masri, S., Smyth, A., Anderson, J.: Adaptive methods for identification of hysteretic structures. In: American Control Conference, ACC95, Seattle, WA (1995)
12. Chassiakos, A., Masri, S., Smyth, A., Caughey, T.: On-line identification of hysteretic systems. ASME J. Appl. Mech. **65**, 194–203 (1998)
13. Chatzi, E.N., Smyth, A.W.: The unscented Kalman filter and particle filter methods for nonlinear structural system identification with non-collocated heterogeneous sensing. Struct. Control Health Monit. **16**, 99–123 (2009)
14. Chatzi, E.N., Smyth, A.W., Masri, S.F.: Experimental application of on-line parametric identification for nonlinear hysteretic systems with model uncertainty. Struct. Saf. **32**(5), 326–337 (2010)
15. Derkevorkian, A., Hernandez-Garcia, M., Yun, H.B., Masri, S.F., Li, P.: Nonlinear data-driven computational models for response prediction and change detection. Struct. Control Health Monit. **22**(2), 273–288 (2015)
16. Derkevorkian, A., Masri, S.F., Fujino, Y., Siringoringo, D.M.: Development and validation of nonlinear computational models of dispersed structures under strong earthquake excitation. Earthq. Eng. Struct. Dyn. **43**, 1089–1105 (2014)
17. Dominguez, A., Sedaghati, R., Stiharu, I.: A new dynamic hysteresis model for magnetorheological dampers. Smart Mater. Struct. **15**, 1179–1189 (2006)

18. Erlicher, S., Point, N.: Thermodynamic admissibility of Bouc–Wen type hysteresis models. C. R. Mec. **332**, 51–57 (2004)
19. Ewins, D.J.: Modal Testing: Theory, Practice and Application, 2nd edn. Research Studies Press LTD, Baldock (2000)
20. Ghanem, R., Romeo, F.: Wavelet-based approach for model and parameter identification of non-linear systems. Int. J. Non-Linear Mech. **36**, 835–859 (2001)
21. Hoshiya, M., Saito, E.: Structural identification by extended Kalman filter. ASCE J. Eng. Mech. **110**(12), 1757–1772 (1984)
22. Ibrahim, S.: Efficient random decrement computation for identification of ambient responses. In: Proceedings of the 19th IMAC, Orlando, FL, pp. 678–703 (2001)
23. Ismail, M., Ikhouane, F., Rodellar, J.: The hysteresis Bouc–Wen model, a survey. Arch. Comput. Methods Eng. **16**, 161–188 (2009)
24. Iwan, W.: A distributed-element model for hysteresis and its steady-state dynamic response. ASME J. Appl. Mech. **33**, 893–900 (1966)
25. Iwan, W., Cifuentes, A.: A model for system identification of degrading structures. Earthq. Eng. Struct. Dyn. **14**, 877–890 (1986)
26. Iwan, W., Lutes, L.: Response of the bilinear hysteretic system to stationary random excitation. J. Acoust. Soc. Am. **43**, 545–552 (1968)
27. James, G., Carne, T., Lauffer, J.: The natural excitation technique (NExT) for modal parameter extraction from operating structures. Int. J. Anal. Exp. Modal Anal. **10**(4), 260–277 (1995)
28. Jayakumar, P., Beck, J.L.: System identification using nonlinear structural models. In: Structural Safety Evaluation Based on System Identification Approaches, pp. 82–102. Springer Fachmedien, Wiesbaden (1988)
29. Jennings, P.: Periodic response of a general yielding structure. J. Eng. Mech. Div. ASCE **90**, 131–166 (1964)
30. Kerschen, G., Poncelet, F., Golinval, J.C.: Physical interpretation of independent component analysis in structural dynamics. Mech. Syst. Signal Process. **21**, 1561–1575 (2007)
31. Kerschen, G., Worden, K., Vakakis, A., Golinval, J.C.: Past, present and future of nonlinear system identification in structural dynamics. Mech. Syst. Signal Process. **20**, 505–592 (2006)
32. Kosmatopoulos, E., Polycarpou, M., Christodoulou, M., Ioannou, P.: High-order neural network structures for identification of dynamical systems. IEEE Trans. Neural Netw. **6**, 422–431 (1995)
33. Kosmatopoulos, E., Smyth, A., Masri, S., Chassiakos, A.: Robust adaptive neural estimation of restoring forces in nonlinear structures. ASME J. Appl. Mech. **68**, 880–893 (2001)
34. Li, S., Suzuki, Y., Noori, M.: Identification of hysteretic systems with slip using bootstrap filter. Mech. Syst. Signal Process. **18**, 781–795 (2004)
35. Lin, J.W.: Adaptive identification of structural systems by training artificial neural networks. Adv. Inf. Sci. Serv. Sci. **4**, 10–17 (2012)
36. Lin, J.W., Betti, R.: On-line identification and damage detection in non-linear structural systems using a variable forgetting factor approach. Earthq. Eng. Struct. Dyn. **33**, 419–444 (2004)
37. Lin, J.W., Wu, T.H.: Modeling and assessment of VWNN for signal processing of structural systems. Struct. Eng. Mech. **45**, 53–67 (2013)
38. Loh, C., Chung, S.: A three-stage identification approach for hysteretic systems. Earthq. Eng. Struct. Dyn. **22**, 129–150 (1993)
39. Ma, F., Zhang, H., Bockstedte, A., Foliente, G., Paevere, P.: Parameter analysis of the differential model of hysteresis. ASME J. Appl. Mech. **71**, 342–349 (2004)
40. Masri, S.: Forced vibration of the damped bilinear hysteretic oscillator. J. Acoust. Soc. Am. **57**, 106–113 (1975)
41. Masri, S., Caffrey, J., Caughey, T., Smyth, A., Chassiakos, A.: A general data-based approach for developing reduced-order models of nonlinear MDOF systems. Nonlinear Dyn. **39**, 95–112 (2005)
42. Masri, S., Caughey, T.: A nonparametric identification technique for nonlinear dynamic problems. ASME J. Appl. Mech. **46**, 433–447 (1979)
43. Masri, S., Miller, R., Saud, A., Caughey, T.: Identification of nonlinear vibrating structures; part I: formulation. ASME J. Appl. Mech. **109**, 918–922 (1987)
44. Masri, S., Miller, R., Saud, A., Caughey, T.: Identification of nonlinear vibrating structures; part II: applications. ASME J. Appl. Mech. **109**, 923–929 (1987)
45. Masri, S., Miller, R., Traina, M., Caughey, T.: Development of bearing friction models from experimental measurements. J. Sound Vib. **148**, 455–475 (1991)
46. Masri, S., Tasbihgoo, F., Caffrey, J., Smyth, A., Chassiakos, A.: Data-based model-free representation of complex hysteretic MDOF systems. Struct. Control Health Monit. **13**, 365–387 (2006)
47. MATLAB and Neural Network Toolbox: Release 2014b. TheMathWorks, Inc., Natick, MA (2014)
48. Peeters, B., De Roeck, G.: Stochastic system identification for operational modal analysis: a review. J. Dyn. Syst. Meas. Control **123**, 659–667 (2001)
49. Pei, J., Smyth, A., Kosmatopoulos, E.: Analysis and modification of Volterra/Wiener neural networks for the adaptive identification of non-linear hysteretic dynamic systems. J. Sound Vib. **275**, 693–718 (2004)
50. Peng, C., Iwan, W.: An identification methodology for a class of hysteretic structures. Earthq. Eng. Struct. Dyn. **21**, 695–712 (1992)
51. Pi, Y., Mickleborough, N.: Modal identification of vibrating structures using ARMA model. ASCE J. Eng. Mech. **115**, 2232–2250 (1989)
52. Smyth, A., Masri, S., Chassiakos, A., Caughey, T.: On-line parametric identification of MDOF nonlinear hysteretic systems. ASCE J. Eng. Mech. **125**, 133–142 (1999)
53. Smyth, A., Masri, S., Kosmatopoulos, E., Chassiakos, A., Caughey, T.: Development of adaptive modeling techniques for non-linear hysteretic systems. Int. J. Non-linear Mech. **37**, 1435–1451 (2002)
54. Smyth, A.W., Masri, S.F., Caughey, T.K., Hunter, N.F.: Surveillance of mechanical systems on the basis of vibration signature analysis. ASME J. Appl. Mech. **67**, 540–551 (2000)
55. Toussi, S., Yao, J.: Hysteretic identification of existing structures. J. Eng. Mech. Div. ASCE **109**, 1189–1202 (1983)
56. Van Overschee, P., De Moor, B.: Subspace Identification for Linear Systems: Theory-Implementation-Application. Kluwer, Dordrecht (1996)

57. Vinogradoc, O., Pivovarov, L.: Vibrations of a system with nonlinear hysteresis. J. Sound Vib. **111**, 145–152 (1986)
58. Wen, Y.: Method for random vibration of hysteretic systems. J. Eng. Mech. Div. ASCE **102**, 249–263 (1976)
59. Wen, Y.: Equivalent linearization for hysteretic systems under random excitation. ASME J. Appl. Mech. **47**(1), 150–154 (1980)
60. Wu, M., Smyth, A.: Real-time parameter estimation for degrading and pinching hysteretic models. Int. J. Non-linear Mech. **43**, 822–833 (2008)
61. Wu, M., Smyth, A.W.: Application of the unscented Kalman filter for real-time nonlinear structural system identification. Struct. Control Health Monit. **14**, 971–990 (2007)
62. Wu, T., Kareem, A.: Modeling hysteretic nonlinear behavior of bridge aerodynamics via cellular automata nested neural network. J. Wind Eng. Ind. Aerodyn. **99**, 378–388 (2011)
63. Yang, J., Lin, S., Huang, H., Zhou, L.: An adaptive extended Kalman filter for structural damage identification. Struct. Control Health Monit. **13**(4), 849–867 (2006)
64. Yar, M., Hammond, J.: Modeling and response of bilinear hysteretic systems. J. Eng. Mech. Div. ASCE **113**, 1000–1013 (1987)
65. Yar, M., Hammond, J.: Parameter estimation for hysteretic systems. J. Sound Vib. **117**, 161–172 (1987)
66. Zhang, H., Foliente, G., Yang, Y., Ma, F.: Parameter identification of inelastic structures under dynamic loads. Earthq. Eng. Struct. Dyn. **31**(5), 1113–1130 (2002)